◆ Human Brain Mapping 5:26–47(1997) ◆

Spatial Extension of Brain Activity Fools the Single-Channel Reconstruction of EEG Dynamics

Jean-Philippe Lachaux, Laurent Pezard, Line Garnero, Christophe Pelte, Bernard Renault, Francisco J. Varela, and Jacques Martinerie*

Unité de Psychophysiologie Cognitive, LENA-Centre National de la Recherche Scientifique Unité de Recherche Associéa 654-Université Pierre et Marie Curie, Hôpital de La Salpêtrière, 75651 Paris, France

Abstract: We report here on a first attempt to settle the methodological controversy between advocates of two alternative reconstruction approaches for temporal dynamics in brain signals: the single-channel method (using data from one recording site and reconstructing by time-lags), and the multiple-channel method (using data from a spatially distributed set of recordings sites and reconstructing by means of spatial position). For the purpose of a proper comparison of these two techniques, we computed a series of EEG-like measures on the basis of well-known dynamical systems placed inside a spherical model of the head. For each of the simulations, the correlation dimension estimates obtained by both methods were calculated and compared, when possible, with the known (or estimated) dimension of the underlying dynamical system. We show that the single-channel method fails to reliably quantify spatially extended dynamics, while the multichannel method performs better. It follows that the latter is preferable, given the known spatially distributed nature of brain processes. *Hum. Brain Mapping 5:26–47, 1997.*
© 1997 Wiley-Liss, Inc.

Key words: nonlinear dynamics; spatially extended systems; EEG; single-channel reconstruction; multichannel reconstruction; correlation dimension; spatiotemporal chaos; coupled map lattices

INTRODUCTION

Since the eighties, the application of nonlinear dynamic methods to the study of surface recordings (EEG) has provided new insights in experimental and theoretical approaches to brain activity [Jansen and Brandt, 1993; Nandrino et al., 1994]. The present article focuses on a key step shared by all of these methods: the reconstruction of a trajectory that mirrors the evolution of the brain in its phase-space. This crucial step can be performed using two methods based either on single or multiple channel recordings. The single-channel reconstruction has so far been the mainstream approach because of its clear mathematical basis (see ''Reconstruction of dynamics from observations''), but it has led to questionable results when rigorously tested [Theiler and Rapp, 1996; Pritchard and Duke, 1995]. Recent developments in spatiotemporal chaos [Cross and Hohenberg, 1993] suggest that this method is ill-suited for spatially extended activities, and if so, this limitation would constitute a severe limitation for the application of single-channel temporal reconstruction of the EEG. In this paper, we use computer

Contract Grant sponsor: Direction de la Recherche et la Technologie, France. Contract Grant sponsor: Center National de la Recherche Scientifique.

*Correspondence to: Jacques Martinerie, Unité de Psychophysiologie Cognitive, LENA-CNRS URA 654-UPMC Hôpital de La Salpêtrière, 47 Bd. de l'Hôpital, 75651 Paris Cedex 13, France. E-mail: LENAJM@EXT.JUSSIEU.FR

Received for publication 10 December 1996; accepted 13 December 1996

© 1997 Wiley-Liss, Inc.

simulations to investigate whether the single-channel choice is thus limited for the study of EEG, and if so, whether the use of the multichannel method is more appropriate.

RECONSTRUCTION OF A DYNAMICS FROM OBSERVATIONS

Any physical system, such as the brain, can be fully described by the values of a certain number of variables representing its physical properties (e.g., the neurons' firing rate). The state vector is the vector which coordinates are these variables. It represents unambiguously the state of the system and determines a trajectory in the phase-space that accounts for the system's dynamics. Well-known mathematical results have shown that the system's complexity can be inferred from the topology of this trajectory [e.g., Eckmann and Ruelle, 1985]. In contrast, in experimental situations, the exhaustive determination of state variables is not available, and thus the phase-space trajectory is unknown. A partial approximation of the topology must be reconstructed from partial, noisy measurements of the system.

For the same reason, any proper estimation of the experimental signals' complexity needs the reconstruction, from the measurements, of measurement vectors whose evolution over time sketches an object with a similar topology to that of the complete phase-space trajectory. In principle, there are two ways to obtain the coordinates of these vectors: they can either be consecutive values of one time series of measures [Packard et al., 1980; Takens, 1981], or a set of simultaneous independent observations [Guckenheimer and Buzyna, 1983]. The first method is usually called the *single*-channel reconstruction, and the second the *multi*channel reconstruction.

The introduction of reconstruction methods has led to a flurry of reports concerning many different natural systems' phase-space trajectories, typically related to the complexity of the signal: the fractal dimension (an estimation of the number of degrees of freedom of the system), Lyapunov exponents (that quantify its sensitive dependence to initial conditions), and the Kolmogorov entropy (that quantifies the loss of predictability over time) [reviewed in Ott et al., 1994]. In some cases, these indices have proven that specific complex physical signals were not stochastic but chaotic [Guckenheimer and Buzyna, 1983]. In this context, chaos means 1) nonlinearity, 2) a low noninteger dimension (i.e., <5), and 3) a sensitive dependence to initial conditions. The correlation dimension (D_2) has been usually favored as the choice index for signal complexity, since it gives an indication of the number of independent variables of the system and thus allows inference of models.

EEG AND LOW-DIMENSIONAL CHAOS

The previous approach was soon applied also to the brain's signals, in a rapidly expanding literature. The "chaotic" nature of surface cerebral activity was estimated [Rapp et al., 1985, 1989; Babloyantz and Destexhe, 1986], until it was shown that linearly filtered noise could display topological characteristics similar to those of chaotic systems [Rapp et al., 1993]. It turned out that before using the chaos quantification toolkit, the nonlinear aspect of EEG signals had first to be proven. A proper test for nonlinearity was devised [Theiler et al., 1992], consisting of differentiating the signal, by the means of any complexity index, from a set of random time-series with the same linear characteristics as the signal. Its application to the EEG showed that most claims for low-dimensional chaos in the EEG were erroneous [e.g., Pritchard and Duke, 1995].

This episode suggested that the use of nonlinear analysis for the study of EEGs should be done with great care. Nowadays, most authors agree that the correlation dimension of a surface-recorded signal reveals nothing about the "chaotic" nature of the brain. Yet, some authors [Pritchard and Duke, 1995] still conclude that it can permit statistical separation between tasks or pathological states, but even this simpler claim is not that clear since others [Theiler and Rapp, 1996] distrust it. The first "chaos-rush" seems to be over.

SPATIOTEMPORAL CHAOS

So far the physical systems that had been shown to generate chaotic signals were either confined in space or recorded with a single probe, so that reconstruction occurred only in time. Studies of nonlinear *spatially extended* systems revealed the existence of chaotic behaviors in both time and space [e.g., Chaté, 1995]. In such systems, the spatial extension can not be ignored: reciprocal effects circulate between the different regions at a finite speed, and spatial heterogeneity arises [Paladin and Vulpiani, 1994]; the decorrelation between the different parts of the system can result in various spatiotemporal patterns, such as traveling waves and spirals [e.g., Gaponov-Grekhov and Rabinovich, 1992]. To date, the theoretical understanding of spatiotemporal chaos is still in its infancy [Cross and Hohenberg, 1994], and insights on the subject are provided by computer simulations and experimental

observations [Kaneko, 1990; Manneville and Chaté, 1992]. However, it is generally thought that the main techniques used for the quantification of nonspatially-extended systems are not applicable where the spatial dimension is involved [Abarbanel et al., 1993; Lorenz, 1991; Politi et al., 1989]. It is believed in particular that reconstruction techniques must take into account the spatial correlation within the system and require data at different points in space [Cross and Hohenberg, 1993]. Therefore, use of the single-channel method for the quantification of spatially extended systems (such as the brain) is now seriously questioned.

These new findings could explain the repeated failures of the single-channel studies of the EEG to provide reliable results. The brain is certainly a nonlinear, spatially extended system comprising coupled assemblies of neuronal groups [Jansen, 1991]. However, the nonlinearity of the EEG has rarely been observed in a stable and repeated manner using the single-channel reconstruction.

SINGLE-CHANNEL VS. MULTICHANNEL

Since the multichannel reconstruction is based on multiple site recordings and thus takes the system's spatial extension into account, it may constitute an adequate alternative method. Moreover, it is a direct application of the Whitney theorem [Whitney, 1936] which states that an embedding can be obtained from independent time series [see Sauer et al., 1991, for generalization]. Some authors have already begun to apply this reconstruction to EEG signals and have found encouraging results [Dvorak, 1990; Wackermann et al., 1993; Pezard et al., 1994, 1996a and b]. Hence, it is extremely necessary to investigate more precisely the extent to which the multichannel reconstruction could be better-suited than the single-channel for the analysis of EEGs.

In the next section of this paper, we investigate the adequacy of single-channel reconstruction for the study of brain dynamics on a theoretical basis. This leads us to several crucial questions that can be addressed by the means of computer simulations. We then describe the methods used in these simulations, based on the reproduction of the experimental setups used for the characterization of brain dynamics. "Results" will show the multichannel and single-channel reconstructions applied to simulated EEG-like signals, their correlation dimensions, and their relative performance. We conclude with a general discussion.

SINGLE-CHANNEL RECONSTRUCTION AND EEG: AN OVERVIEW

The EEG is the measure of the electrical activity of the neurons [Nunez, 1981] as recorded on the scalp, i.e., after diffusion through the brain, the skull, and the skin. From an electric point of view, the brain may be seen in a first approximation as a collection of dipoles, lying in the cortex and perpendicular to its surface. In this basic framework, it can therefore be fully described at any given time, by the vector of all the dipoles' amplitudes, that we denote $\mathbf{X}(t)$. Each surface-recording measures a potential that is a function of $\mathbf{X}(t)$, so that the EEG signal can be expressed by an n-dimensional vector

$$\mathbf{M}(t) = H(\mathbf{X}(t))(= \{m_1(t), m_2(t), \ldots, m_n(t)\}),$$

where H is the measurement function, and n the number of electrodes.

In dynamical studies, the brain is assumed to be a deterministic dynamical system, such that $\mathbf{X}(t)$ evolves over time according to a nonlinear equation:

$$\partial^n \mathbf{X} / \partial t^n = F_\mu(\partial^{n-1}\mathbf{X} / \partial t^{n-1}, \ldots, \mathbf{X}),$$

where F_μ is its evolution function that depends on a set of parameter μ. These parameters have a functional significance: they determine the response of the system to exogenous or endogenous stimulations. Different parameters may correspond to different conditions of attention, or to different pathologies, for instance. The ambition of nonlinear studies of brain activity is to detect parameter changes from a topological description of the EEG.

QUESTIONS RAISED BY THE SINGLE-CHANNEL RECONSTRUCTION

General framework

The principle of the single-channel reconstruction consists in choosing one electrode i, and building k-dimensional vectors

$$\mathbf{V}_i(t) = \{m_i(t), m_i(t - \tau), \ldots, m_i(t - (k - 1) \times \tau)\},$$

where $m_i(t)$ is the potential recorded at time t and site i, and τ is a number called the delay; k is the embedding dimension.

The potential picked up by an electrode can be viewed as a linear combination of all the activities of

the dipoles' amplitudes. The contribution of each dipole is the product of its amplitude by a weighting coefficient that depends on its position and orientation. If **p** denotes the amplitude of the dipole located in spatial position M and if P expresses the electrode position, then in a coarse approximation, the weighting coefficient can be said to be proportional to $\|\mathbf{PM}\|^{-2} \cdot \cos(\langle \mathbf{p}, \mathbf{PM} \rangle)$. Some of these coefficients can be very small because the dipoles are far from the electrode or badly oriented. Thus, an electrode does not record evenly all the dipoles. This situation is of the utmost importance for the single-channel reconstruction of the EEG. We will call ''close'' the dipoles that contribute mainly to the signal, and ''remote'' those that are far away or badly oriented.

To get a first insight, let's consider a simplified case where the brain is constituted of two uncoupled sets of dipoles: s and s′. These two sets can be described by two state vectors **s**(t) and **s**′(t) whose evolution is defined by two *un*coupled dynamical systems with two correlation dimensions d and d′. The potential measured by the electrode can be considered as a linear combination of the dipoles' amplitudes and can thus be written:

$$M(t) = \mathbf{a} \times \mathbf{s}(t) + \mathbf{b} \times \mathbf{s}'(t)$$

(where × denotes the scalar product and **a** and **b** are two weight vectors). If the coordinates of **a** and **b** are of the same order, then the correlation dimension of the trajectory reconstructed from M(t) using the single-channel method must be roughly equal to the sum of d and d′. On the other hand, if **a** (or **b**) is zero, the expected dimension is d′ (or d). Besides these two obvious cases, it is not clear what to expect. When $\|\mathbf{a}\|$ is much bigger than $\|\mathbf{b}\|$, only a portion of the ''brain'' (s in this case) is actually recorded by the electrode. The measure M(t) can thus be considered a measure of **s**(t) with an additive noise caused by **s**′(t). But what dimension must be expected? In principle, a reconstruction, from M(t), of the system dimension should yield d + d′, because **s**′(t) is a part of M(t). In experimental situations, we expect that there must be some value of the ratio $\|\mathbf{b}\| / \|\mathbf{a}\|$ under which the value given by the single-channel reconstruction must be an inappropriate approximation of d (because of noise from **s**′(t)).

However, in the brain, the two sets of dipoles are actually coupled by a dense network of connections [e.g., Braitenberg and Schüz, 1991; Friston et al., 1995]. In that situation, the activity of s′ affects the reconstructed dimension either as an additive noise (as described in the previous case), or via the connections with s. According to classic mathematical results [Takens, 1981], the dynamics of a set of n coupled variables can be reconstructed from any measure of these variables, e.g., the observation of only one of these variables. Thus, the dimension reconstructed by any electrode should in theory be that of the entire system. In practical situations, even when s and s′ are coupled, it is nevertheless the case that the effect provoked by s′ fools the dimension estimate made from the surface electrode. In that case, the dimension estimation is encumbered by two difficulties: the noise from the remote dipoles, and the methodological limitation related to the computation of correlation dimension in spatially extended systems.

Can the single-channel reconstruction be used for global quantification of brain dynamics?

A second issue to discuss is whether in practical situations, the ''exact'' value of the dimension reconstructed from an electrode should be that of the entire brain (global quantification), or that of the region that is close to where recording is made (local quantification).

Suppose that the single-channel method reconstructs the dynamic of the whole brain. A logical consequence is that the estimated dimension should not depend on the position of the recording site. But this is not what is reported in the EEG literature: in most papers [e.g., Pritchard and Duke, 1992] the dimension varies with the electrode; this has even led some authors to draw dimension maps based on interpolation to account for this effect [Pritchard and Duke, 1992]. Such variations can be due to the two factors mentioned previously (the additive noise from the remote dipoles and the methodological drawbacks related to the spatial extension of the brain). The extent of the noise effect depends on whether the additive noise caused by the remote dipoles is sufficient to induce important variations of the correlation dimension across the electrodes.

To understand the influence of spatial extension, one must bear in mind that, in spatially extended systems, there is a degree of spatial decorrelation between the regions [Cross and Hohenberg, 1993], i.e., signals propagate between the different parts of the system at a finite speed. In the brain, such phenomena occur since the propagation speed of the action potentials from neuron to neuron is finite; this could lead to a decorrelation between the dimension measures of the different electrodes. Thus, one must show how the spatial extension is an additional cause of variations of the dimension estimate across the electrodes.

Can single-channel reconstruction be used for local quantification of brain dynamics?

The alternative to global quantification is the estimation of the complexity of only a region of the brain. As previously mentioned, the brain, as a dynamical system, can be said to be governed by an equation of the type:

$$\partial^n \mathbf{X} / \partial t^n = F_\mu(\partial^{n-1}\mathbf{X} / \partial t^{n-1}, \ldots, \mathbf{X}).$$

As part of the global system, a region of the brain is fully characterized by a local state vector $\mathbf{X}_1$, a projection of $\mathbf{X}$, such that its complement $\mathbf{X}_2$ describes the state of the other parts of the system. $\mathbf{X}$ may be written

$$\mathbf{X} = (\mathbf{x}_1 + \mathbf{x}_2).$$

It follow that:

1. The phase-space trajectory of the region of interest is no more than a projection of the phase-pace trajectory of the global system. And thus, there is no guarantee that the trajectory of the subsystem is unfolded. If this trajectory intersects itself, it means that the state of the subsystem at any given time cannot be unambiguously deduced from the previous state; thus the signal behaves in a noise-like manner and there is no point in measuring its correlation dimension.
2. The variables that are external to the subsystem act as parameters on its evolution function, such that:

$$\partial^n \mathbf{x}_1 / \partial t^n = F^1_\mu(\partial^{n-1}\mathbf{X} / \partial t^{n-1}, \ldots, \mathbf{X}) = G_{\mu,x_2}(\partial^{n-1}\mathbf{x}_1 / \partial t^{n-1}, \ldots, \mathbf{x}_1)$$

(F^i_μ denotes the restriction of F_μ to the subspace related to $\mathbf{X}_1$). Since there are no reason why $\mathbf{X}_2$ should be a constant, the parameters of the subsystem's evolution function $G_{\mu,x2}$ are changing, and the system is not invariant. However, the invariance of the system is a major requirement before computing its correlation dimension [Jansen, 1991].

The previous arguments suggest that the quantification of the dimension of a subsystem is very risky. However, in some very limited cases, it might be possible to quantify regional complexities. It is known that spatially extended systems can present regions that apparently isolate themselves from the rest of the system to adopt a coherent structure (cluster) with its own degree of complexity [Kaneko, 1990]. Furthermore, since the couplings between neurons do not always decrease with the distance that lies between them, the cells of a coherent group may be sparsely distributed throughout the cortex. Thus, two separate situations must be studied to decide if the single-channel is well-suited to quantify meaningful local complexity indices: when the electrode records only one cluster, or when it measures the sum of several clusters' activities.

Summary

This section is mostly based on the observation that the potential recorded by an electrode is the sum of two terms: the contribution of a small ''magnified'' set of dipoles that lie under the recording site and point toward the electrode, and the contribution of the other remote dipoles. This observation raises five crucial questions which will be addressed by five numerical simulations:

- Question 1: To which extent do the contributions of remote dipoles (acting as a noise source) fool the estimates of the dimension?
- Question 2: Are the variations of dimension obtained between different electrodes due to the noise-like contribution of the remote dipoles?
- Question 3: Are these variations due to an intrinsic inability of the single-channel reconstruction to deal with spatially extended dynamics?
- Question 4: Can the single-channel reconstruction provide information on local complexity when the cortex falls into well separated clusters of coherent activity?
- Question 5: Can the single-channel reconstruction provide information on local complexity when these clusters of coherent activity are not well-separated in space?

CHOICE OF SIMULATIONS AND NUMERICAL METHODS

Generating EEG-like signals

All the simulations proceed basically the same way and are fully explained in this section. A model human head is defined by three concentric spherical shells representing the brain, the skull, and the skin with their respective conductivity, and a set of dipoles is

placed inside the inner shell (the brain). The dipoles evolve according to dynamical laws chosen to address the five questions just listed. The potential is then computed on several points of the scalp, and this "EEG" is investigated using single-channel and multichannel reconstruction. The correlation dimension is computed for each channel in the first case, and for the global recording in the second case.

Model of diffusion

The evaluation of scalp potentials generated by cortical dipoles in realistic models of the head is a largely unsolved problem, known as the "forward problem" [Renault and Garnero, 1995]. This problem has an exact analytic solution in the simplified case where the head is modeled by concentric spheres of isotropic and homogenous conductivities. This model may present some flaws when precise forward computation is required, although it provides an excellent basis for our study, since it takes into account spatial diffusion of the dipoles' fields and mirrors the fact that transmission across successive layers does not affect the Fourier spectrum of the signals (at least for the frequencies of our signals [Nunez, 1981]).

We thus considered three concentric shells representing the brain (radius, 8.5 cm; conductivity, 1 (arbitrary unit)), the skull (radius, 9.2 cm; conductivity, 0.0128), and the skin (radius, 10 cm; conductivity, 1), and we placed dipoles inside the inner shell. A set of positions (the electrode sites) was chosen on the surface of the outer shell, and the potential generated by the dipoles on the electrodes was calculated using developments in spherical harmonics [de Munck, 1988].

In the following, we considered Oxyz to be the following perpendicular axis: O is the center of the spheres, Ox is the axis pointing toward the nose, Oy points toward the left ear, and Oz points to the vertex. Any vector $\mathbf{u}$ will be referred to by its spherical coordinates (r, θ, φ), $r = \|\mathbf{u}\|$, $\theta = (Oz, \mathbf{u})$, and $\varphi = (Ox, \mathbf{u}^{xy})$ ($\mathbf{u}^{xy}$ is the projection of $\mathbf{u}$ on the Oxy plane (Fig. 1).

The field computed from the dipoles represents the potential difference, induced by the dipoles, between the scalp and any position far from the dipoles. It therefore mimics, to a first approximation, an EEG with linked-ears or collar reference. Some authors [e.g., Stam et al., 1996] have used the mean potential over all the electrodes as reference. As explained in appendix B, using this reference is equivalent to studying a modified dynamic of the dipoles, different from that of the original.

Models of the "brain"

Our purpose is to investigate the influence of the *spatial extension* of brain dynamics on the performance of two reconstruction techniques (single-channel and multichannel). Recent sophisticated models of real brain dynamics can be found in the literature [e.g., Nunez, 1995], but we limit ourselves here to spatially extended, mathematically exact models. This is necessary since only exactly characterized dynamics permit us to *isolate* the effects of spatial extension while providing the means to estimate dynamical indices (such as the analytic formulation of the Lyapunov spectra, an approximation of the correlation dimension). In consequence, we devised a series of simulations to answer the five questions raised above.

Each case studied was defined by: 1) the choice of a dynamical system whose variables were sampled over 8,192 time steps as dipole amplitudes, 2) the positions and orientations of the dipoles, and 3) the positions of the electrodes (this information can be found in detail in Tables I–III).

The choice of the number of time steps (8,192 points) allows computation of dimensions as high as 9 ($\approx 2 \times \log(8{,}192)$ [Eckmann and Ruelle, 1992]); this is also the maximum dimension that can be reconstructed with the multichannel method in EEG experiments with 20 electrodes (since the theory [Whitney, 1936] states that $2d + 1$ measures are needed to reconstruct a trajectory of dimension d and thus $2 \times \underline{9} + 1 < 20$).

The following is an overview of the different simulations designed to answer the five questions mentioned in the first section.

Question 1: To what extent does the contribution of remote dipoles fool the dimension computation (simulation TORUS)?

Two orthogonal dipoles were placed in the same central position inside the brain, and their amplitudes were set to evolve independently from each other in a periodic manner. The dimension of each dipole's system was one, but the dimension of the sum of the two systems was two. Nineteen electrodes were evenly arrayed on a quarter of a ring contained in the plane defined by the dipoles (see Fig. 6a). In this configuration, each electrode's potential received different relative contributions of the two dipoles: the extreme electrodes 1 and 19 were located to catch the activity of only one of the dipoles, and we expected to find a correct dimension of 1 from these sites; we also expected to find a correct dimension of 2 for the middle electrode that received an equivalent contribu-

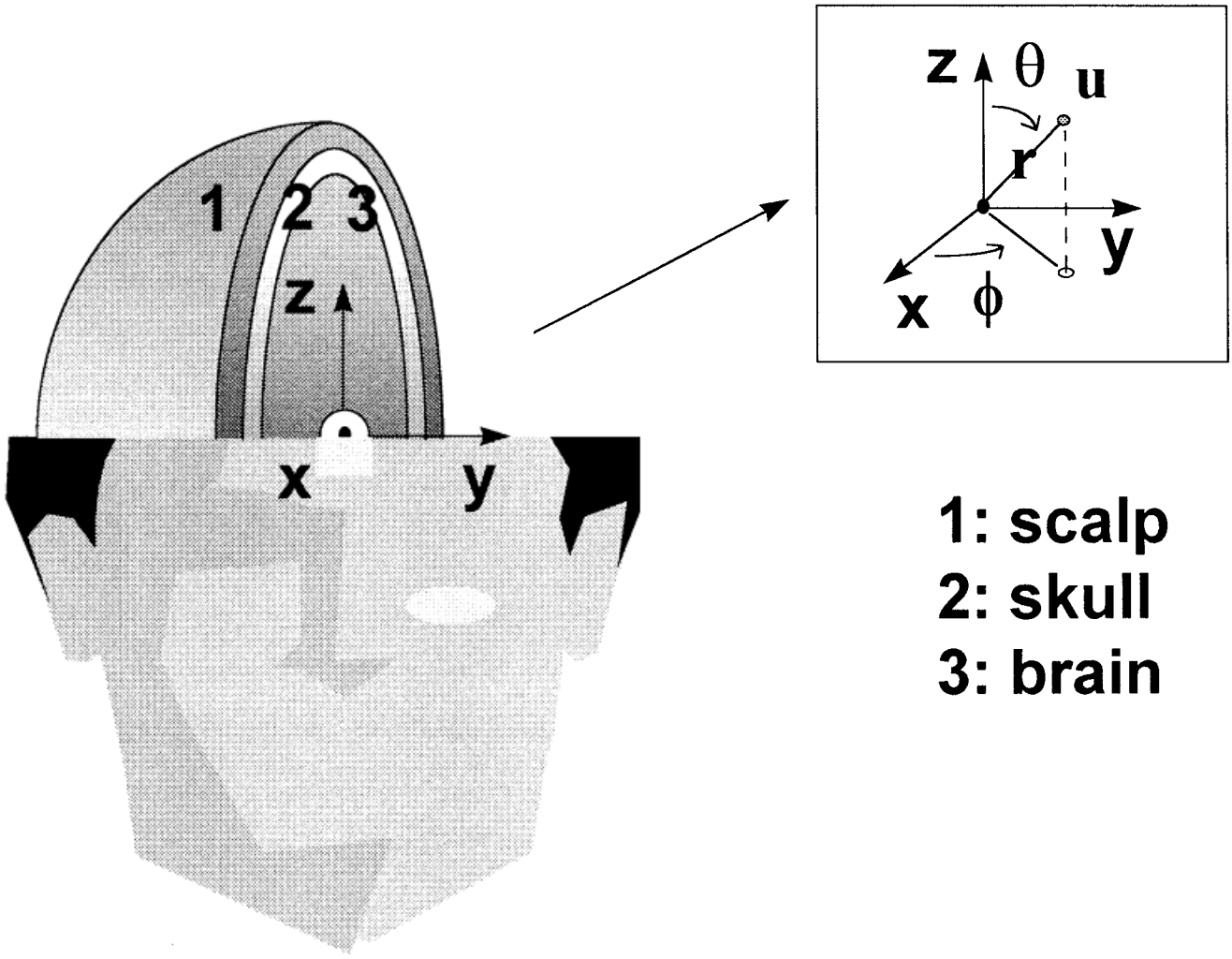

Figure 1.
Head is modelled by three concentric spherical shells with homogenous and isotropic conductivities.

tion from the two dipoles. But theory is of little help as to what one should find at the other recording sites.

Question 2: When recording a globally coupled network of dipoles, can the variations of dimension obtained for different electrodes be explained by the noise-like contribution of the remote dipoles (simulation LORENZ)?

Three orthogonal dipoles were placed in the same central position. They were recorded by 19 electrodes placed according to the 10–20 international electrode placement system [Jasper, 1958] (see Table III). The Lorenz system [Lorenz, 1963] was integrated using the Runge-Kutta fourth-order method with a step of 0.01. After the first 1,000 transients had been discarded, the system was allowed to evolve over 5 × 8,192 time steps, and every five steps the value of the three variables was taken as dipole amplitudes; this procedure provided a time series of 8,192 amplitudes for each dipole. The system was chosen because of its simplicity and because its correlation dimension was known (2.06). If any electrode did not render the correct dimension, it would mean that the activity of (at least) one of the dipoles had acted as a noise on the measure.

Question 3: Are the variations of dimension obtained between different electrodes due to an intrinsic inability of the single-channel reconstruction to deal with spatially extended dynamics (simulation CML)?

Coupled map lattices (CML) were considered in this case. The coupled map lattices are some of the best-known and simplest systems to exhibit spatiotemporal chaos [Kaneko, 1990]. These systems are discontinuous

TABLE I. Equations used as brain models

TORUS
$x(t) = \cos(t)$
$y(t) = \cos(\exp(1).t)$
LORENZ
$\dot{x}(t) = 10.(y(t) - x(t))$
$\dot{y}(t) = -x(t).z(t) + 28.x(t) - y(t)$
$\dot{z}(t) = -x(t).y(t) - (8/3).z(t)$
CML
$x_i(t) = (1 - \epsilon).f(x_i(t)) + (\epsilon/2).(f(x_{i-1}(t)) + f(x_{i+1}(t)))$
$i \in (1, N)$, "$x_0(t)$" = $x_N(t)$ and "$x_{N+1}(t)$" = $x_1(t)$ (periodic boundaries)
$f(x) = 1 - a.x^2$ (logistic function)
$\epsilon = 0.3$ and $a = 1.9$
CLUSTER (1 and 2)
$x_i(t) = (1 - \epsilon).f(x_i(t)) + (\epsilon/2).(f(x_{i-1}(t)) + f(x_{i+1}(t)))$
$i \in (1, N)$, "$x_0(t)$" = $x_N(t)$ and "$x_{N+1}(t)$" = $x_1(t)$ (periodic boundaries)
$f(x) = 1 - a.x^2$ (logistic function)
$\epsilon = 0.22$ and $a = 1.65$

TABLE III. Electrode positions for each of the simulations

TORUS

Electrode	Position
Electrode (i) ($i \in (1, 19)$)	$\theta = 60°, \phi = (i - 1).5°$

LORENZ and CML

Electrode	Position	Electrode	Position
Fpz	$\theta = 90°, \phi = 0°$	C3	$\theta = 45°, \phi = 90°$
Fp2	$\theta = 90°, \phi = 342°$	T7	$\theta = 90°, \phi = 90°$
Fp1	$\theta = 90°, \phi = 18°$	T6	$\theta = 90°, \phi = 234°$
F8	$\theta = 90°, \phi = 306°$	P4	$\theta = 62°, \phi = 216°$
F4	$\theta = 62°, \phi = 324°$	Pz	$\theta = 45°, \phi = 180°$
Fz	$\theta = 45°, \phi = 0°$	P3	$\theta = 62°, \phi = 144°$
F3	$\theta = 62°, \phi = 36°$	T5	$\theta = 90°, \phi = 126°$
F7	$\theta = 90°, \phi = 54°$	O2	$\theta = 90°, \phi = 198°$
T8	$\theta = 90°, \phi = 270°$	Oz	$\theta = 90°, \phi = 162°$
C4	$\theta = 45°, \phi = 270°$	O1	$\theta = 90°, \phi = 180°$
Cz	$\theta = 0°, \phi = 0°$		

CLUSTER (1 and 2)

Electrode	Position
Electrode (i, j) ($i \in (1, 10)$) ($j \in (1, 20)$)	$\theta = ((11 - i)/10).90°$, $\phi = ((j - 1)/20).360°$
Electrode (201)	$\theta = 0°, \phi = 0°$

in time and space but continuous in amplitude. They can produce a variety of behaviors that covers most of the known aspects of spatiotemporal chaos. Their dynamics are determined by two parameters: the strength of the couplings (ϵ, see Table I) between the elements of the network, and the degree of nonlinearity (a, see table I) of the evolution function (f, see table I) of the elements (see Fig. 2).

These parameters were set to get a state of fully developed turbulence ($\epsilon = 0.3$ and $a = 1.9$). In this case, the dimension (computed from the Lyapunov spectrum) could roughly be approximated by $d = 0.75 \times N$ (where N denotes the number of elements

TABLE II. Dipole positions and orientations

Dipoles	Orientation	Position	Amplitude
TORUS			
Dipole 1	$\theta = 90°, \phi = 0°$	$r = 0.5, \theta = 0°, \phi = 0°$	x(t)
Dipole 2	$\theta = 90°, \phi = 90°$	$r = 0.5, \theta = 0°, \phi = 0°$	y(t)
LORENZ			
Dipole 1	$\theta = 90°, \phi = 0°$	$r = 0.5, \theta = 0°, \phi = 0°$	x(t)
Dipole 2	$\theta = 90°, \phi = 90°$	$r = 0.5, \theta = 0°, \phi = 0°$	y(t)
Dipole 3	$\theta = 0°, \phi = 0°$	$r = 0.5, \theta = 0°, \phi = 0°$	z(t)
CML			
Dipole (i, j) ($i \in (1, Nt)$) ($j \in (1, Np)$)	Radial to scalp	$r = 0.8, \theta = ((Nt + 1 - i)/Nt) . 90°, \phi = ((j - 1)/Np) . 360°$	$x_{N_p \cdot (i-1)+j}$
Dipole N	Radial to scalp	$r = 0.8, \theta = 0°, \phi = 0°$	$x_N(t)$
CLUSTER (1 and 2)			
Dipole (i, j) ($i \in (1,7)$) ($j \in (1, 28)$)	Radial to scalp	$r = 0.8, \theta = ((8 - i)/7) . 90°, \phi = ((j - 1)/28) . 360°$	See text
Dipole 197	Radial to scalp	$r = 0.8, \theta = 0°, \phi = 0°$	See text

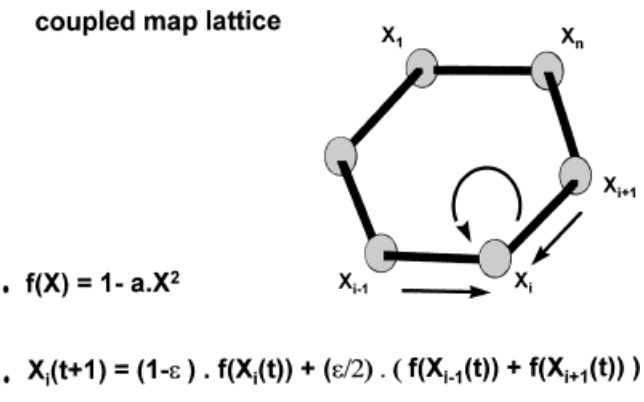

Figure 2.
Architecture of a coupled map lattice (CML) with n automata (periodic boundaries and nearest-neighbors coupling; see **Question 3** for details).

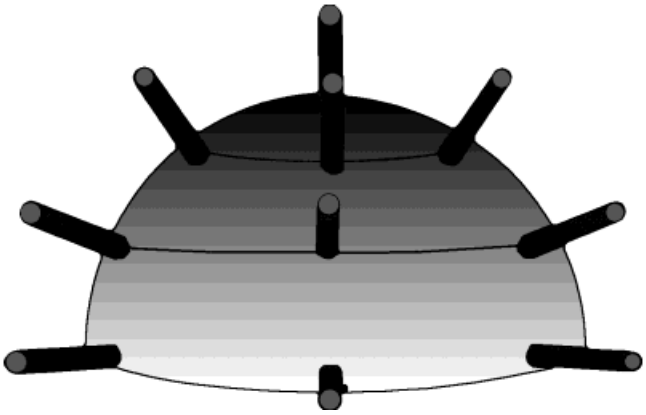

Figure 3.
Dipole positions in the CML and CLUSTER (1 and 2) simulations. Dipoles (bars) are radial to the cortex surface (sphere), and evenly distributed on circles.

in the lattice). We considered nearest-neighbor couplings to benefit from a vast literature in which the correlation dimension has often been computed [Bauer et al., 1993].

We simulated systems of increasing correlation dimensions by increasing the number of elements N in the network (N = 7, 13, 19, 25, 37, 65, 101, 197, 401, 901, 1,601, 10,001). This provided a practical way to assess the reliability of the reconstruction techniques when spatially extended systems of increasing complexity are considered. For each of them, dipoles were evenly placed on N_t circles lying in planes parallel to the ear-nose plane (Oxy); N_p dipoles were evenly positioned on each circle (see Fig. 3). An additional dipole was placed at the vertex, so that $N = N_t \times N_p + 1$ (the different values of Nt and Np can be found in Table IV). The values of the N variables of the lattices were taken over 8,192 time steps (after discarding 1,000 transients). The electrode positions were the same as for the Lorenz system.

Questions 4 and 5: Can the single-channel reconstruction provide information on local complexity when the cortex falls into clusters of coherent activity a) separated in space (question 4) and b) mingled (question 5) (simulations CLUSTER1 (for question 4) and CLUSTER2 (for question 5))?

To judge from the capacity of the single-channel method to quantify local complexity indices, we considered two systems of dipoles made from the same coupled map lattice (CLUSTER1 and CLUSTER2). By choosing a lower coupling strength than in the previous example ($\epsilon = 0.22$) and a lower degree of nonlinearity ($a = 1.65$), we were able to generate spatial inhomogeneities within a lattice of 197 automata. Inside the network, activities ranging from quasiperiodicity to much higher complexity (see Fig. 4) could be observed.

To quantify a degree of complexity for each automata, we devised a ''pseudoentropy'' function called ''occupation.'' The ''occupation'' value of automata was computed from the time series of its activity: this time series was first normalized, so that its distribution was included in the $[-1, +1]$ interval with a standard deviation of 1. The interval was then divided into 1,000 boxes (B_i, ($i \in [1; 1{,}000]$)), so that each box contained a certain proportion $p(B_i)$ of the normalized time-series data points. The occupation function of the time series was finally defined as

$$-\sum_{B_i} p(B_i) \times \ln (p(B_i)).$$

TABLE IV. Dipole distributions for CML simulation

Value of N	Nt: number of crowns	Np: number of dipoles per crown
7	2	3
13	2	6
19	3	6
25	3	8
37	3	12
65	4	16
101	5	20
197	7	28
401	10	40
901	15	60
1,601	20	80
10,001	50	200

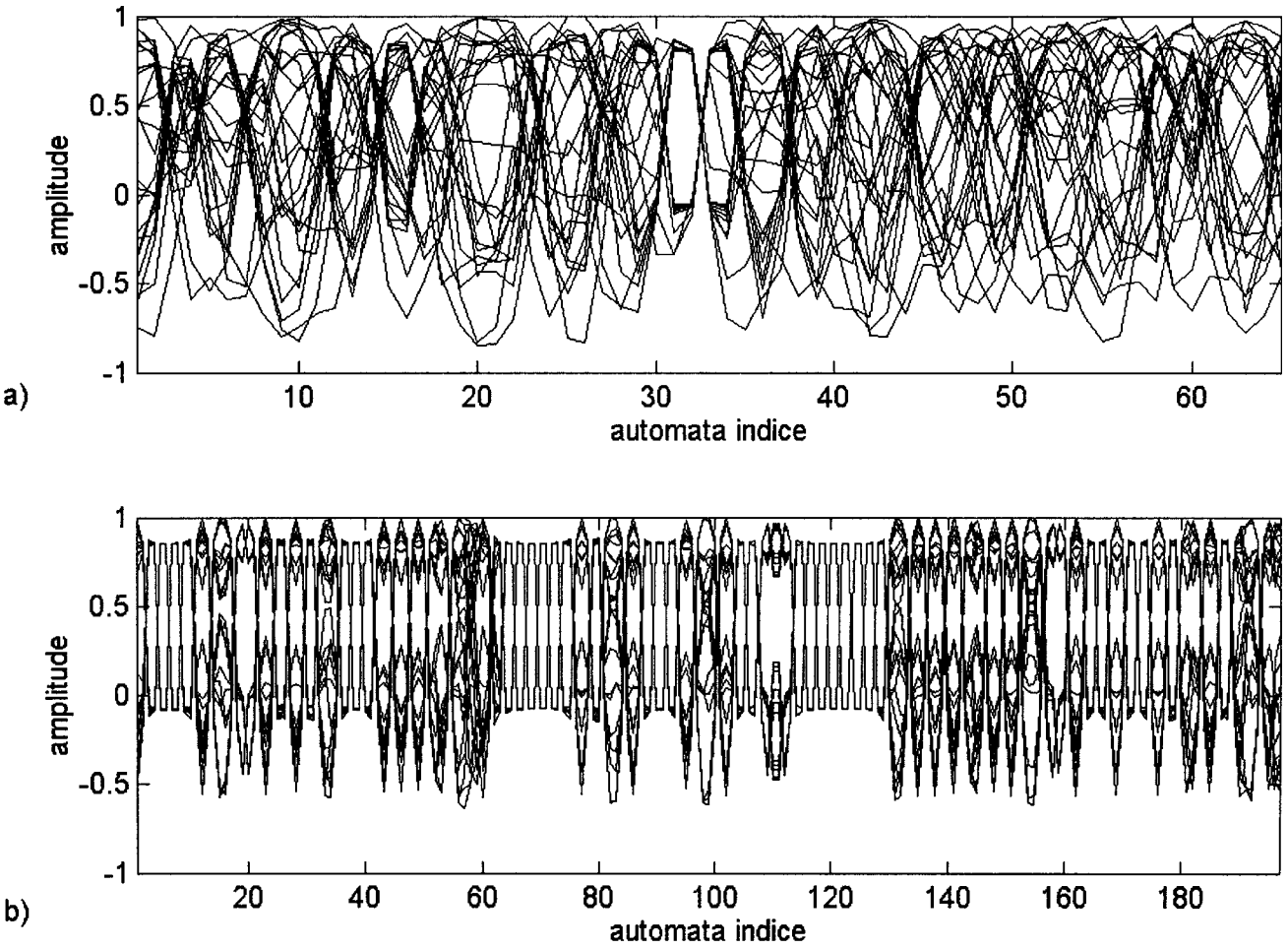

Figure 4.

Behavior of two coupled map lattices. **a:** a = 1.9, ϵ = 0.3, N = 65. **b:** a = 1.65, ϵ = 0.22, N = 197. Graphs represent superposition over 25 time steps of different runs of the function x(i) where x(i) is the amplitude of the i-th automata of the lattice. **a:** Chaos is homogenous in space. **b:** Clusters with quasiperiodic behavior seem to decorrelate from the rest of the network.

It follows that quasiperiodic automata had a low ''occupation'' level. Using this procedure, it was possible to define the ''occupation'' value of a dipole's amplitudes or of the potentials recorded by an electrode.

Several radial dipoles (197) were placed on seven crowns and their activity was measured by 201 electrodes evenly distributed on the scalp's surface. All automata were ranked according to their ''occupation'' level. Using this ranking, we attributed the automata's activities to the dipoles in two different fashions to devise two simulations. In CLUSTER1, low ''occupation'' activities were grouped in a closed region of the cortex to form a single cluster of dipoles with quasiperiodic motion. In CLUSTER2, no attention was paid to the ranking when attributing the amplitudes to the dipoles; quasiperiodic dipoles were distributed throughout the cortex. The ''occupation'' maps corresponding to those two systems are depicted in Figure 5. These simulations allowed us to investigate the two cases where one dynamical extended system fell into a) small *separated* subsystems with homogenous complexities (CLUSTER1), and b) mingled coherent clusters (CLUSTER2).

Quantification of dynamics

The dynamics were reconstructed using both multichannel and single-channel methods.

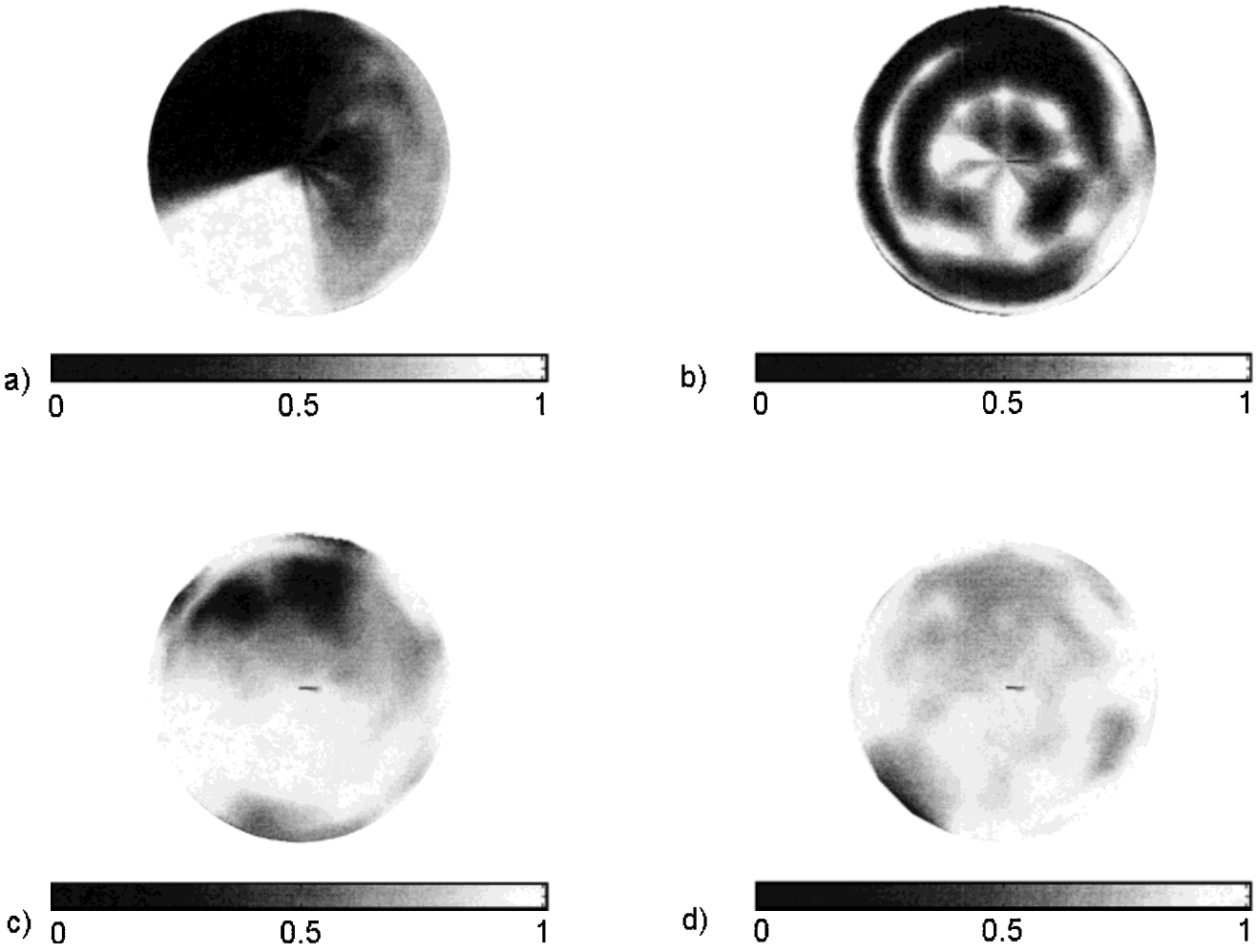

Figure 5.

''Occupation'' maps for the simulations CLUSTER1 and CLUSTER2. **a:** Occupation value has been computed for each of the 197 dipoles of the CLUSTER1 network, and then interpolated on the whole cortex. Figure represents top view of the resulting map. A cluster of low ''occupation'' is clearly seen. **b:** Corresponding map on the scalp's surface, calculated from the ''occupations'' of the 201 recorded electrode potentials. A diffusion of high ''occupation'' levels can be observed, although a region of low ''occupation'' remains. Same maps are represented for CLUSTER2 (**c:** dipoles; **d:** electrodes). In CLUSTER2, clusters of low ''occupation'' level exist, but they are not as segregated as in CLUSTER1. Therefore, ''occupation'' map d is much more homogenous than b.

Single-channel reconstruction

We applied the single-channel reconstruction by choosing one electrode i, and building k-dimensional vectors

$$\mathbf{V}_i(t) = \{m_i(t), m_i(t - \tau), \ldots, m_i(t - (k - 1) \times \tau)\},$$

where ($m_i(t)$ is the potential recorded at time t and site i, and τ is a number called delay; k is the embedding dimension). The value of τ was chosen using the geometrical method of Rosenstein et al. [1994].

Multichannel reconstruction

Multichannel reconstruction consists in building k-dimensional vectors

$$\mathbf{V}(t) = \{m_1(t), m_2(t), \ldots, m_k(t)\},$$

where $m_i(t)$ is the potential recorded at time t and site i, and k is the embedding dimension.

In order to get fair estimates of the correlation dimension, it is required that the reconstructed trajectory has the same topological properties as the original

d-dimensional phase-space trajectory. In practical cases, there must be a one-to-one correspondence between the points of the two curves. A sufficient condition for that is derived from Whitney's theorem

$$(k \geq 2d + 1).$$

This condition is sufficient but not necessary; in this study it is possible to be a little more precise, since the measurement functions are known: for the multichannel reconstruction, the topology is preserved (in general) when k is greater than the dimension of the phase-space (a proof can be found in Appendix A). In the case of the coupled map lattices, for instance, the correlation dimension d of the systems equals 75% of the number N of automata; Whitney's criteria suggests taking

$$k = 2 \times 0.75 \times N + 1 = 1.5 \times N + 1,$$

but $k > N$ may be enough, as explained in Appendix A.

Dimension estimation

We estimated the correlation dimension following the classic procedure of Grassberger and Procaccia [1983] with the correction of Theiler [1986]. We computed D_2 for increasing values of the embedding dimension after singular value decomposition (SVD), and worked in a reduced space where the variance of each singular value was $>10^{-3}$; this threshold did not affect the D_2 value [Albano et al., 1988], but filtered the noise.

In principle, the correlation dimension increases and then reaches a saturation plateau when the orbit is unfolded. When *no saturation* was observed, we took it as a sign that the trajectory was not unfolded and we did not consider D_2 as a reliable quantity.

For some systems, it was possible to calculate the theoretical dimension using the Lyapunov spectrum and the Kaplan-Yorke conjecture [Kaplan and Yorke, 1979]. For this purpose we implemented an algorithm using QR decomposition [Eckmann and Ruelle, 1992] to compute the Lyapunov exponents and the Lyapunov dimension of the systems. We took the results with caution, since this formula does not apply when the sum of the Lyapunov exponents is positive; this is never the case in natural phenomena, but it appears for certain parameters of the CML (Coupled Map Lattices). When possible, we computed this value and used it to evaluate the performance of the reconstruction.

Testing for nonlinearity

Since dynamical methods may be biased by linearly correlated noise [Rapp et al., 1993], the validity of the correlation dimension is usually tested by the comparison between the values computed on raw data and those computed on surrogate data with the same linear properties (power spectrum, autocorrelation function). In the case of single-channel reconstruction, surrogate data are obtained by randomizing the phases in the Fourier domain [Theiler et al., 1992]. In the case of multichannel recording, multivariate surrogate data were used to preserve crosscorrelation between channels [Prichard and Theiler, 1994]. The procedure thus consisted in testing the H_o hypothesis that the correlation dimension had been obtained from linearly correlated noise. To do so, a set of 39 surrogate data (either uni- or multivariate) was generated and the distance between the raw measurement and the mean of the surrogates was computed

$$(S = \Delta m / \sigma).$$

If S was roughly superior to 2, the measurement obtained for raw data differed significantly from the data obtained with surrogate data (at a significance level of 5%: two-tailed t-test at 2.5%). This estimate was used to decide whether the H_o hypothesis should be rejected. Since the underlying dynamics were presumed to be nonlinear, it was of particular interest to see how the dimension of the measurement space affected the estimated degree of nonlinearity. Thus, our aim was triple. We wanted 1) to have an idea of the reliability of the dimension indices that we measured, 2) to investigate the relative abilities of single-channel and multichannel models to detect nonlinearities, and 3) to test the variations of the nonlinearity index with the embedding dimension.

RESULTS

TORUS

Single-channel reconstruction

Dimension estimation. The reconstructed dimension varied with the location of the electrode. For electrodes 1 and 19, the reconstructed dimension was 1.1 (see Fig. 6b); this value was almost correct, since only one of the two dipoles was recorded by those electrodes. Elec-

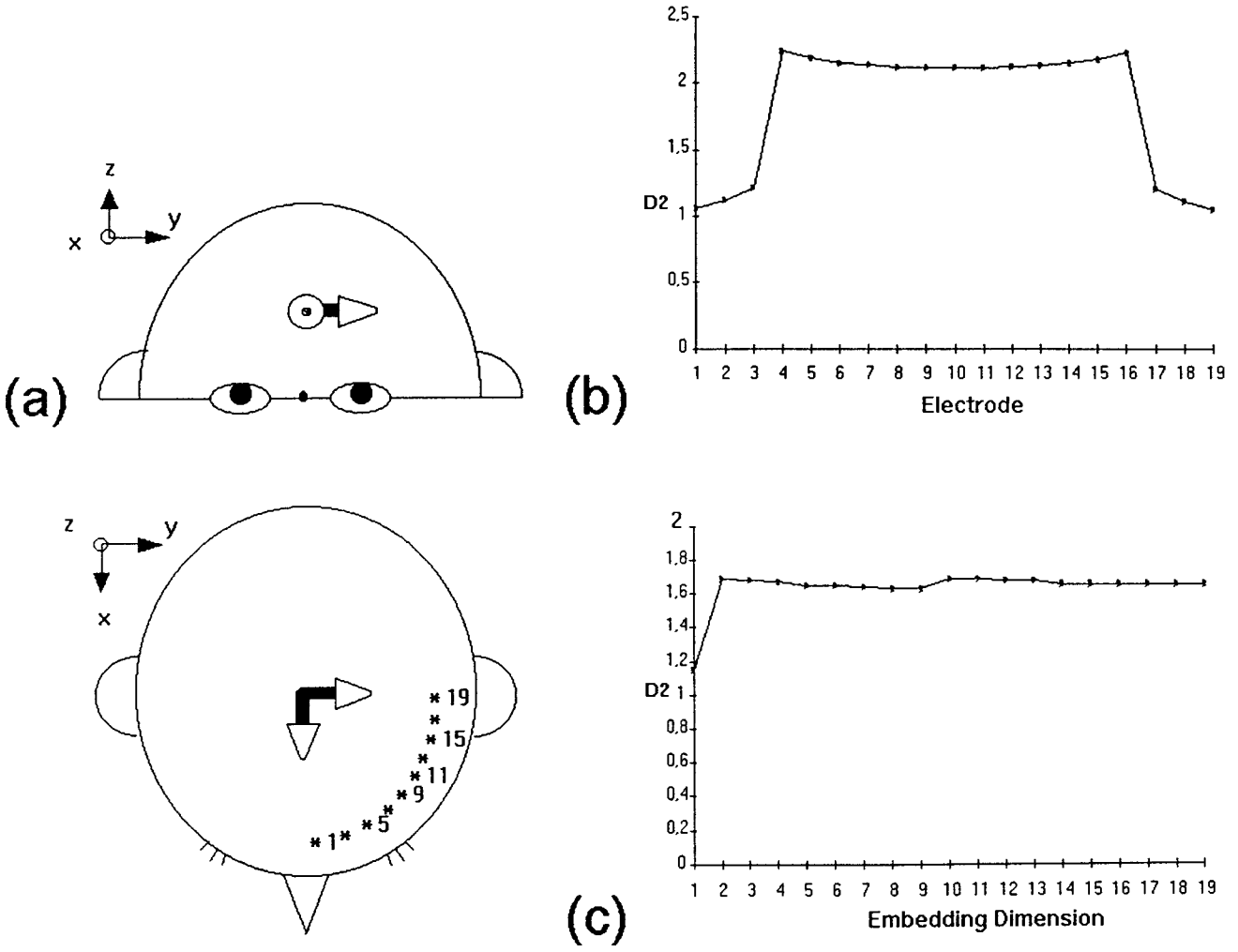

Figure 6.

TORUS simulation. **a:** Frontal and top view of head, representing locations of the two dipoles and the 19 electrodes. **b:** Single-channel correlation dimension, calculated for each of the 19 recording sites. **c:** Presentation of multichannel correlation dimension D2, as a function of the embedding dimension.

trodes 2, 3, 17, and 18 also led to a dimension estimation close to 1, while they recorded both dipoles. This underestimation of the actual estimation of the system (2.0) is easy to explain: for each of these electrodes, only one of the dipoles contributed in a significant manner to the recorded potential. However, the dimension estimation is not that of a single dipole; a slight variation was induced by the other dipole. Two regions of the scalp can be defined, over which electrodes fail to reconstruct the two-dimensional dynamic of the dipoles' system. These regions have a very sharp and well-defined border. All electrodes leading out of them produced a fair estimation of the system's dimension.

Nonlinearity. All recorded potentials were markedly different from their surrogates.

Multichannel reconstruction

Dimension estimation. A saturation of the correlation dimension estimate D2 was observed when increasing the spatial embedding (Fig. 6c). This saturation value (1.7) was less than the exact dimension (2.0) of the system. This underestimation can be explained by an insufficient number of data points (only 8,192): the density of points was not large enough in the reconstruction space for the recon-

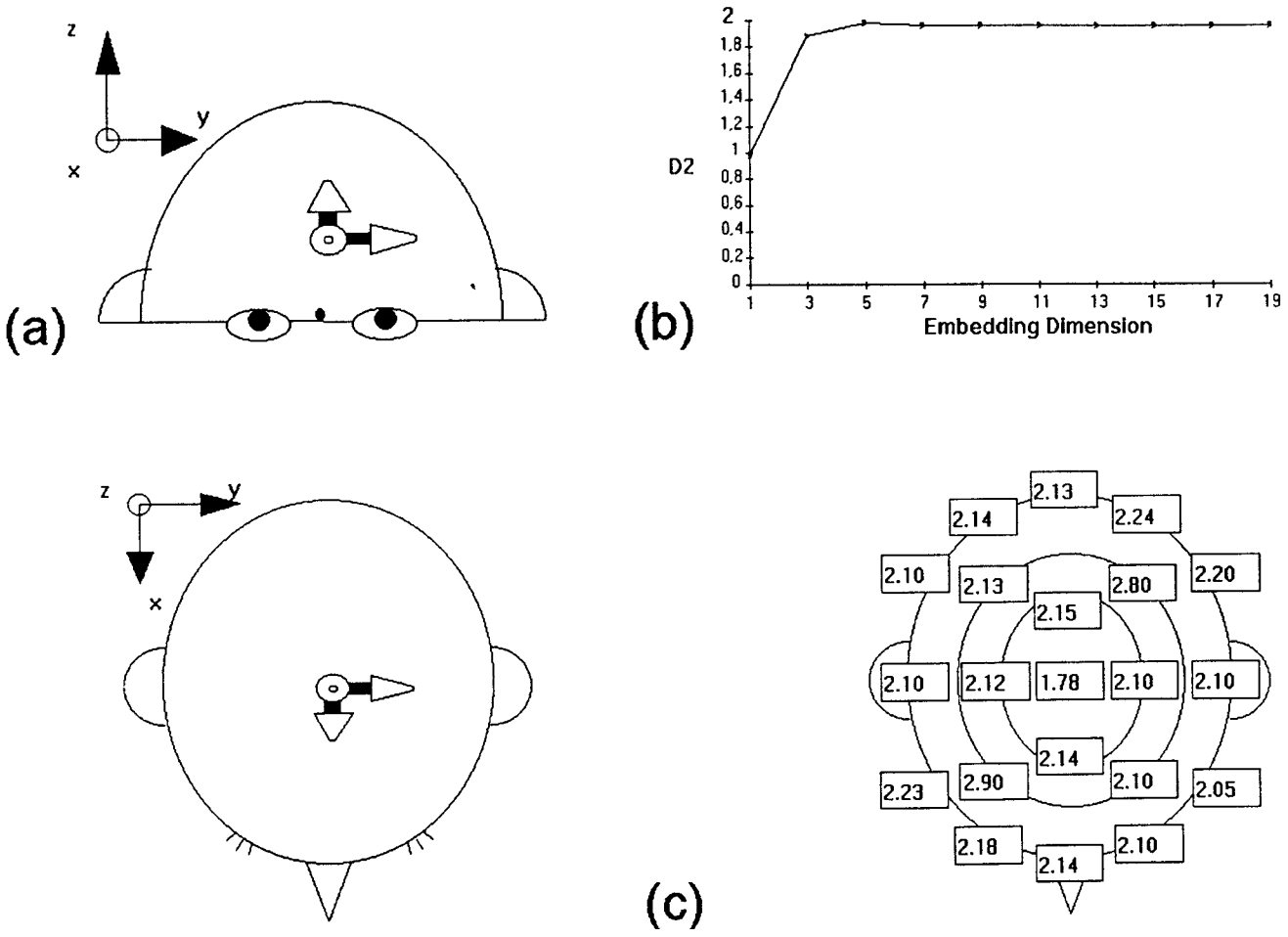

Figure 7.
LORENZ simulation. **a:** Frontal and top view of head, representing locations of the three dipoles. **b:** Presentation of multichannel correlation dimension D2, as a function of the embedding dimension. **c:** Single-channel correlation dimension, calculated for each of the 21 recording sites.

structed trajectory to evenly fill a two-dimensional subspace.

Nonlinearity. For spatial embeddings >1, the signal differed significantly from its surrogates.

LORENZ

Single-channel reconstruction

Dimension estimation. A dimension estimate could be calculated for all recording sites (see Fig. 7c). These values showed notable variations across electrodes, certainly because the sets of data points were finite. Despite this variability and contrary to the previous simulation, all electrodes described the dynamic of the whole system. This effect could clearly be attributed to the couplings between the three dipoles.

Nonlinearity. For all electrodes, the nonlinearity of the signal was significant.

Multichannel reconstruction

Dimension estimation. The multichannel reconstructed dimension was saturated with increasing spatial embedding (Fig. 7b). The value obtained (1.96) is close to the actual dimension of the underlying system (2.06).

Nonlinearity. For spatial embeddings >2, the signal differed significantly from that of its surrogates.

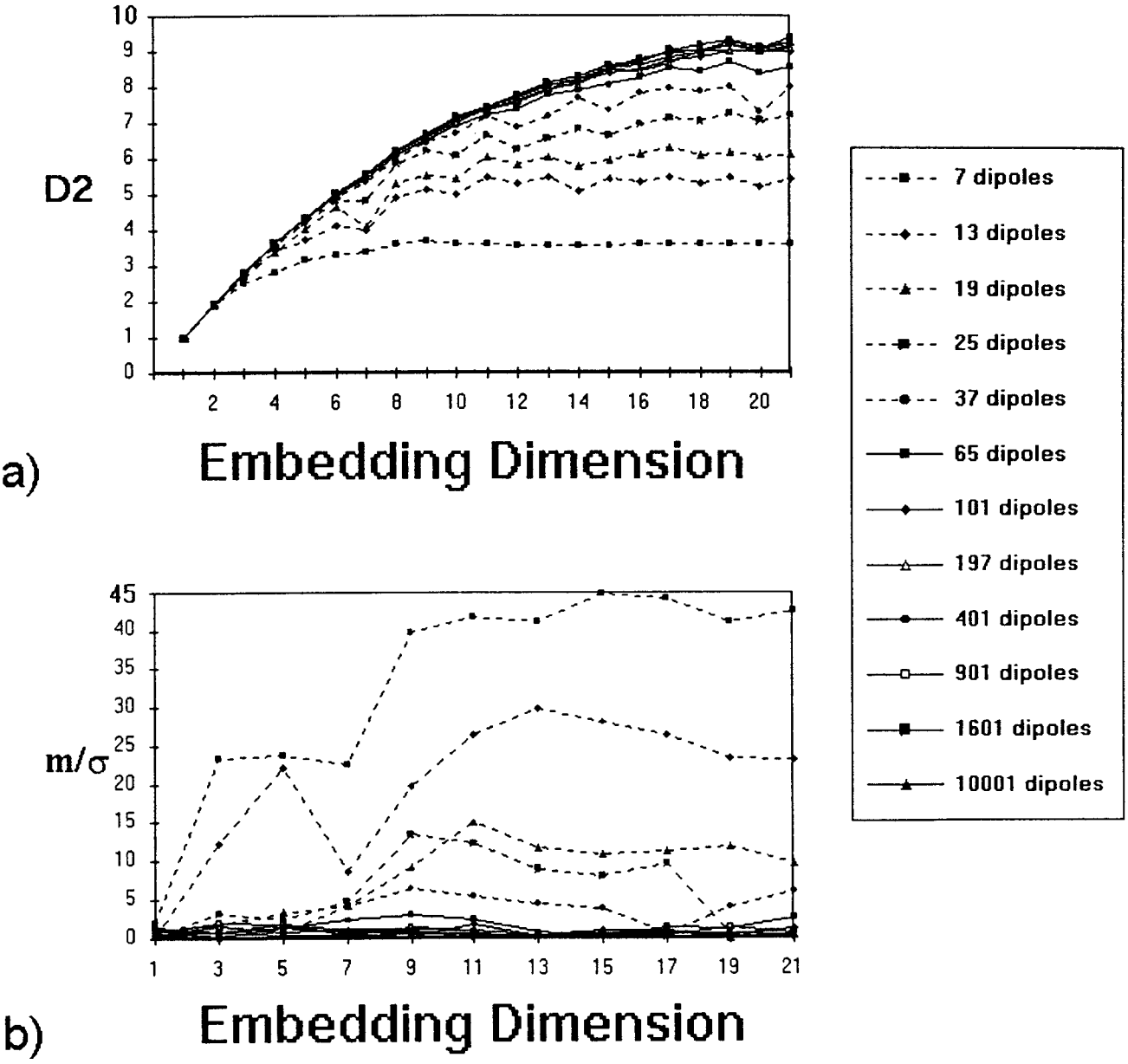

Figure 8.
CML simulations: multichannel reconstruction. Representation, for all lattices, of the correlation dimension D2 **(a)** and the m/σ value **(b)** as a function of the embedding dimension.

CML

Single-channel reconstruction

Dimension estimation. For all lattices and all electrodes, the correlation dimension increased as a function of the embedding dimension, showing no saturation. Therefore no dimension estimation could be derived from single-channel reconstruction.

Nonlinearity. Since no dimension could be computed, it was not possible to compute the difference with the surrogates.

Multichannel reconstruction

Dimension estimation. A saturation of dimension was observed for all lattices when enlarging the spatial embedding (Fig. 8). The reconstructed dimension ap-

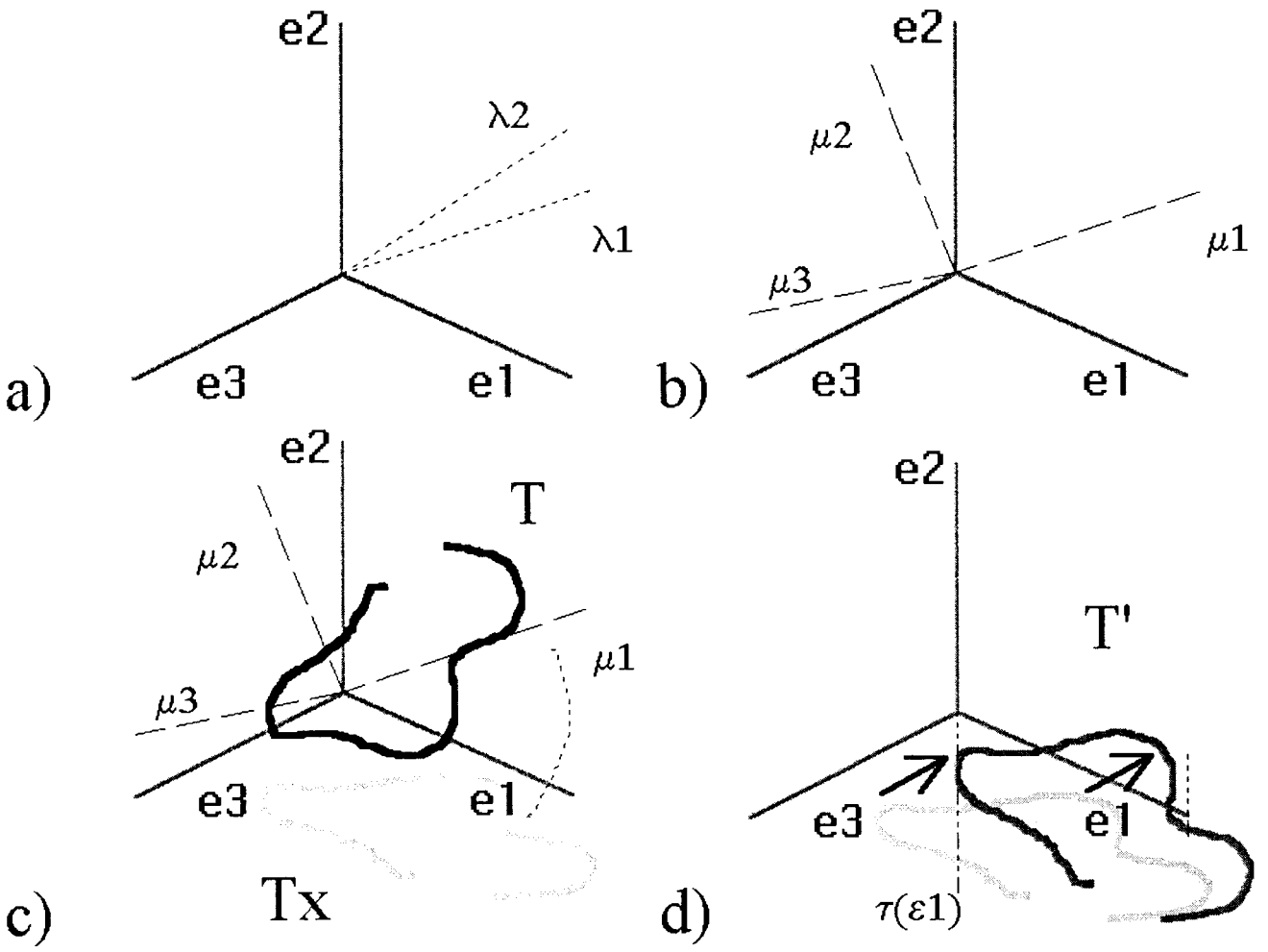

Figure 9.

Transformations leading from the brain's phase-space trajectory to the EGG. **a:** Vectors ($\lambda_1, \lambda_2, \ldots, \lambda_m$) are computed from source-to-scalp coefficients. **b:** Orthonormal basis ($\mu_1, \mu_2, \ldots, \mu_p$) is then constructed. **c:** T is rotated using the tranformation ρ (Tx). **d:** Tx is projected down to the subspace $\langle e_1, e_2, \ldots, e_r \rangle$ ($r = 2$, here). The EEG is then deduced from the resulting trajectory.

peared to increase with the size of the lattice, as suggested by the Lyapunov dimension's computations (0.75× (size of the lattice)). However, a saturation of the reconstructed dimension with the lattice size was observed: no dimension was >10. Dimensions of the large lattices (>65 dipoles) were not reliable; this was confirmed by investigation of the nonlinearity of the signals. Note that even for the small lattices, the correlation dimensions found using the Grassberger-Procaccia algorithm (GPA) are low, as compared to their Lyapunov dimensions. Similar differences have been reported in previous studies [e.g., Bauer et al., 1993] and were attributed to a limitation of the GPA.

Nonlinearity. For all lattices >65 dipoles, the EEG was not distinguishable from linearly correlated noise, and it confirmed that their low-dimension estimations made no sense. On the contrary, the multichannel reconstruction enabled us to show that lattices with <37 dipoles had a low-dimensional, nonlinear, and chaotic behavior.

CLUSTER1 and CLUSTER2

Single-channel reconstruction

Dimension estimation. For both simulations we chose six electrodes to reconstruct the dynamic of the underlying system. To make this choice, we ranked all electrodes' potentials according to their "occupation" function. The first three and the last three were selected (the last electrodes correspond to the darkest areas of

Fig. 5c, d). As for the previous simulation, none of the electrodes led to a saturation of the correlation dimension with the embedding dimension.

Nonlinearity. Since no dimension could be computed, it was not possible to compute the difference with the surrogates.

Multichannel reconstruction

Dimension estimation. A saturation plateau was reached for both CLUSTER1 and CLUSTER2 simulations. For CLUSTER1, with an embedding dimension of 25, the estimated dimension was 5.19; it was slightly higher for CLUSTER2, at 6.08.

Nonlinearity. As for the estimation of the dimension both signals (CLUSTER1 and CLUSTER2) significantly differed from those of their surrogates.

DISCUSSION AND CONCLUDING REMARKS

We are now in the position of bringing some answers to the question of the application of the single-channel reconstruction to the EEG and to compare its performance with the multichannel reconstruction.

Comparison of the two reconstruction techiques

The simulation TORUS confirmed that when a dipole is ill-located or ill-oriented with respect to an electrode position, its contribution to the measured potential fools the dimension estimate on that electrode. The electrodes that received a much stronger activity from one of the dipoles than from the other did not provide reliable value of ''complexity.'' The dimension obtained was ''halfway'' between the dimension of the dominant system and the dimension of the global system. Is this quantification completely meaningless? The LORENZ simulation showed that this effect could induce variations of the dimension estimate, even with a globally coupled dynamical system of dipoles. However, such variations were small and a rough estimation of the system's dimension could still be obtained. This conclusion did not hold when the system was spatially distributed, as demonstrated by the CML simulation: the spatial extension fooled the single-channel reconstruction, even for small lattices.

If global quantification is impossible, can the single-channel reconstruction properly quantify local complexity indices? The theoretical study suggested that this was possible only if the brain behaved as a collection of coherent and rather independent sets of dipoles. Since there were no reasons why such clusters should lie in separate parts of the brain, the CLUSTER2 simulation was devised to investigate whether a local quantification was possible when coherent sets were mixed. This is not possible: no saturation plateau of the dimension could be obtained from any electrode. The last situation was when the clusters were segregated in space, and was addressed by CLUSTER1, and the results showed no improvement in the saturation, as compared with CLUSTER2.

In conclusion, our simulations support the contention that *the single-channel reconstruction is not adapted for a local or global quantification of the brain's dynamics.* The multichannel technique performed better for our simulations and seems better adapted to characterize global spatiotemporal dynamics. However, this conclusion was drawn from artificial signals; its extension to real physiology is based on the fact that these signals are orignated within a realistic model of the head, are propagated as if they were real brain signals, and have time and intensity scales within physiological ranges. To use a realistic brain model (e.g. Babloyontz and Destexhe, 1933) with known dynamical properties would be, it seems, a task beyond the means available today [Nunez, 1995]. It also follows that we cannot conclude whether the multichannel reconstruction technique is actually *optimal* for brain studies, but only that it is an improvement on single-channel.

Fooling reconstructions

It is important to notice that high-dimensional systems systematically fool the multichannel (and a fortiori the single-channel) methods. When the reconstruction space is too small to contain a topological equivalent of the phase-space trajectory of the system, our results indicate that the dimension estimate is no longer reliable. From the surrogate data analysis, it is clear that when the dimensionality of the system increases (e.g., CML) for a fixed embedding dimension, the index m/σ decreases, which means that the signal becomes progressively indistinguishable from linearly-correlated noise, as the reconstructed trajectory twists onto itself. It is better unfolded when the ratio between the phase-space orbit and the measurement space dimension is close to one; but when this ratio increases the number of crossings within the reconstructed orbit rises and the unfolded parts get smaller. Finally, the measurements at one time-step carry no more information on the next measurements, and the recorded signal acts like noise. This is supported by recent results of Politi et al. [1989], who showed that when considering n contiguous automata

in an N-variables coupled map lattice (similar to that studies in this paper), the correlation dimension of the subsystem is n (provided that n is small as compared to N). Our study suggests that the phase-space trajectory of the n-automata subsystem is no more than a projection of the global system phase-space trajectory and presumably contains multiple crossings; therefore, its correlation dimension should be that of an n-variables stochastic system, which is n.

The problem is that taken as a whole, the brain is likely to be of too high a dimensionality to be unfolded in a 21-measures multichannel space. A recent method, called false nearest strands [Liebert et al., 1991] permits us to test this claim by a systematic search of overlap trajectories which are not detected when the embedding dimension is progressively increased. A first application to neural signals gave us some encouraging results [Müller-Gerking et al., 1996].

In our opinion, a number of theoretical advances will be needed for further analysis of the brain's dynamics. First, for a proper assessment of an EEG's nonlinear or deterministic origin, a new type of surrogate data that does not attempt to distinguish between nonlinear [Theiler et al., 1992] or deterministic (''DVS'') [Kaplan and Glass, 1992] dynamics and linear noise, but rather between twisted nonlinear deterministic dynamics and linear noise. Secondly, a systematic study of the robustness of classic topological indices should also be done; this should lead to new topological indices that would be preserved between the phase-space trajectory and its reconstructed image, even when it is folded, i.e., a ''rumple-proof'' index as it were. Third, new tools should be adapted to the quantification of spatiotemporal chaos since the brain is, above all, a spatially extended system.

Embedding dimension

When the embedding dimension of the reconstruction space is too small, the signal generated by the brain's high-dimensional dynamics cannot be distinguished from linear noise. In this case the computation of the correlation dimension on such signals is meaningless, and the obstacle can only be solved by increasing the embedding dimension. This can be done by considering larger sets of electrodes, but at some point, the measurements become redundant. This stresses the usefulness of recording, for example, the magnetic component of brain signals (MEG) along with the EEG, to get additional information. Another possibility is to combine the single-channel and multichannel techniques and to use successive measurements of several electrodes to represent the state of the system. This method is very promising and permits us to increase easily the embedding dimension. However, high embedding dimensions impose heavy computational costs.

ACKNOWLEDGMENTS

This work was financed in part by a grant from the Direction de la Recherche et la Technologie, France, and by general support from Centre Natioanl de la Recherche Scientifique. We thank J. Müller-Gerking for many helpful discussions. We are also grateful to the anonymous referees for their comments and corrections.

REFERENCES

Abarbanel HD, Brown R, Sidorowich JJ, Tsimring LS (1993): The analysis of observed chaotic data in physical systems. Rev Mod Physics 65:1331–1392.

Albano AM, Muench J, Schwartz C, Mees AI, Rapp PE (1988): Singular value decomposition and the Grassberger-Procaccia algorithm. Physical Review A 38:3017–3028.

Babloyantz A, Destexhe A (1986): Low-dimensional chaos in an instance of epilepsy. Proc Natl Acad Sci USA 83:3513–3517.

Babloyantz A, Destexhe A (1993): Nonlinear analysis and modelling of cortical activity. In: Demongeot J, Capasso R (eds): Mathematics Applied to Biology and Medicine. Winnipeg: Wuerz Publishing, pp 35–48.

Bauer M, Heng H, Martienssen W (1993): Characterization of spatiotemporal chaos from time series. Phys Rev Lett 74:521–524.

Braitenberg V, Schüz A (1991): Anatomy of the Cortex. Statistics and Geometry. Berlin: Springer-Verlag.

Chaté H (1995): On the analysis of spatio-temporally chaotic data. Physica D 86:238–247.

Cross MC, Hohenberg PC (1993): Pattern formation outside of equilibrium. Rev Mod Physics 65:851–1112.

Cross MC, Hohenberg PC (1994): Spatio-temporal chaos. Science 263:1569–1570.

De Munck JC (1988): The potential distribution in a layered anisotropic spheroidal volume conductor. J Appl Physiol 64:464–470.

Dvorak I (1990): Takens versus multichannel reconstruction in EEG correlation exponent estimates. Phys Lett 151:225–233.

Eckmann JP, Ruelle D (1985): Ergodic theory of chaos and strange attractors. Rev Mod Physics 57:617–656.

Eckmann JP, Ruelle D (1992): Fundamental limitations for estimating dimensions and lyapunov exponents in dynamical systems. Physica D 56:185–187.

Friston KJ, Tononi G, Sporns O, Edelman GM (1995): Characterising the complexity of neuronal interactions. Hum Brain Mapping 3:302–314.

Gaponov-Grekhov AV, Rabinovich MI (1992): Nonlinearities in Action. Oscillations, Chaos, Order, Fractals. Berlin: Springer-Verlag.

Grassberger P, Procaccia I (1983): Measuring the strangeness of strange attractors. Physica D 9:189–208.

Guckenheimer J, Buzyna G (1983): Dimension measurements for geotrophic turbulence. Phys Rev Lett 51:1438–1441.

Jansen BH (1991): ''Is it?'' and ''So what?''—A critical view of EEG chaos. In: Duke DW, Pritchard WS (eds): Measuring Chaos in the Human Brain. Singapore: World Scientific, pp 83–96.

Jansen BH, Brandt ME (1993): Nonlinear Dynamical Analysis of the EEG. Singapore: World Scientific.

Jasper H (1958): The ten twenty electrode system of the international federation. Electroencephalogr Clin Neurophysiol 10:371–375.

Kaneko K (1990): Clustering, coding, switching, hierarchical ordering and control in network of chaotic elements. Physica D 41:137–172.

Kaplan D, Glass L (1992): Direct test for determinism in a time series. Physical Rev Lett 68:427–430.

Kaplan JL, Yorke JA (1979): Chaotic behavior of multidimensional difference equations. In: Peitgen HO, Walter HO (eds): Functional Differential Equations and Approximation of Fixed Points. Lecture Notes in Mathematics 730. Berlin: Springer-Verlag, p 204.

Liebert W, Pawelzik K, Schuster HG (1991): Optimal embeddings of chaotic attractors from topological considerations. Europhys Lett 14:521.

Lorenz EN (1963): Deterministic nonperiodic flow. J Atmospheric Sci 20:130–141.

Lorenz EN (1991): Dimension of weather and climate attractors. Nature 353:241–244.

Manneville P, Chaté H (1992): Collective behaviors in spatially extended systems with local interactions and synchronous updating. Prog Theor Physics 87:1–60.

Müller-Gerking J, Neuenschwander S, Martinerie J, Pezard L, Renault B, Varela FJ (1996): Detecting non-linearities in neuroelectrical signals: A study of synchronous local field potentials. Physica D 94:65–91.

Nandrino JL, Pezard L, Martinerie J, El Massioui F, Renault B, Jouvent R, Allilaire JF, Widlöcher D (1994): Decrease of complexity in EEG as a symptom of depression. Neuroreport 5:528–530.

Nunez PL (1981): Electric Fields of the Brain. New York: Oxford University Press.

Nunez PL (1995): Neocortical Dynamics and Human EEG Rhythms. New York: Oxford University Press.

Ott E, Sauer T, Yorke JA (1994): Coping With Chaos—Analysis of Chaotic Data and the Exploitation of Chaotic Systems. New York: John Wiley & Sons.

Packard NH, Crutchfield JP, Farmer JD, Shaw RS (1980): Geometry from a time series. Physics Rev Lett 45:712–716.

Paladin G, Vulpiani A (1994): Predictability in spatially extended systems. J Phys A Math Gen 27:4911–4917.

Pezard L, Martinerie J, Breton F, Bourzeix JC, Renault B (1994): Non-linear forecasting measurements of multichannel EEG dynamics. Electroencephalogr Clin Neurophysiol 91:383–391.

Pezard L, Martinerie J, Müller J, Varela FJ, Renault B (1996a): Entropy quantification of human brain spatio-temporal dynamics. Physica D 96:344–354.

Pezard L, Nandrino JL, Renault B, El Massioui F, Allilaire JF, Müller J, Varela FJ, Martinerie J (1996b): Depression as a dynamical disease. Biol Psychiatry 39:991–999.

Pezard L, Lachaux JP, Nandrino JL, Adam C, Garnero L, Renault B, Varela FJ, Martinerie J (1997): Local and global entropy quantification in neuronal systems. Acta Physica Pol (in press).

Politi A, D'Alessandro G, Torcini A (1989): Fractal dimensions in coupled map lattices. In: Abraham NB, Albano AM, Passamante A and Rapp PE (eds): Measures of Complexity and Chaos. New York and London. Plenum Press. 409–424.

Prichard D, Theiler J (1994): Generating surrogate data for time series with several simultaneous measured variables. Physics Rev Lett 73:951–954.

Pritchard WS, Duke DW (1992): Dimensional analysis of no-task human EEG using the Grassberger-Procaccia method. Psychophysiology 29:182–192.

Pritchard WS, Duke D (1995): Dimensional analysis of resting human EEG II. Surrogate-data testing indicates nonlinearity but not low-dimensional chaos. Psychophysiology 32:486–491.

Rapp PE, Zimmerman ID, Albano AM, de Guzman GC, Greenbaum NN (1985): Dynamics of spontaneous neural activity in the simian motor cortex: The dimension of chaotic neurons. Phys Letter A 110:335–338.

Rapp PE, Bashore TR, Martinerie JM, Albano AM, Zimmerman ID, Mees AI (1989): Dynamics of brain electrical activity. Brain Topog 2:99–118.

Rapp PE, Albano AM, Schmah TI, Farwell LA (1993): Filtered noise can mimic low dimensional chaotic attractors. Phys Rev E 47:2289–2297.

Rapp PE, Albano AM, Zimmerman ID, Jiménez-Montano MA (1994): Phase-randomized surrogates can produce spurious identifications of non-random structure. Phys Letter A 192:27–33.

Renault B, Garnero L (1995): L'imagerie électromagnétique cérébrale, principe de base et perspectives. In: Instrumentation Physique en Biologie et en Médecine. Paris: Lavoisier, pp 131–139.

Rosenstein MT, Collins JJ, De Luca CJ (1994): Reconstruction expansion as a geometry-based framework for choosing proper delay times. Physica D 73:82–98.

Sauer T, Yorke JA, Casdagli M (1991): Embedology. J Stat Phys 65:579–616.

Stam CJ, Van Woerkom TCAM, Pritchard WS (1996): Use of nonlinear EEG measures to characterize EEG changes during mental activity. Electroencephalogr Clin Neurophysiol 99:214–224.

Takens F (1981): Detecting strange attractors in fluid turbulence. Springer Lect Notes Math 898:366–381.

Theiler J (1986): Spurious dimension from correlation algorithms applied to limited time-series data. Phys Rev A 34:2427–2432.

Theiler J, Rapp PE (1996): Re-examination of the evidence for low-dimensional, nonlinear structure in the human electroencephalogram. Electroencephalogr Clin Neurophysiol 98:213–222.

Theiler J, Eubank S, Longtin A, Galdrikian B, Farmer JD (1992): Testing for nonlinearity in time series: The method of surrogate data. Physica D 58:77–94.

Wackermann J, Lehmann D, Dvorak I, Michel CM (1993): Global dimensional complexity of multi-channel EEG indicates change of human brain functional state after a single dose of a nootropic drug. Electroencephalogr Clin Neurophysiol 86:193–198.

Whitney H (1936): Differentiable manifolds. Ann Math 37:645–680.

APPENDIX A

In the simulations shown in this paper, the correspondence between the phase-space trajectories of the systems, and the trajectories reconstructed from measurements, is known. On the basis of this knowledge, this appendix specifies different conditions under which the topologies of the two trajectories are identical, in the case of multichannel reconstruction.

In other words, if we assume that the phase-space trajectory does not intersect with itself, the one-to-one condition is ensured if and only if the reconstructed trajectory does not have self-crossings. This study investigates the various configurations that lead to such crossings. Since we consider only the multichannel reconstruction, the dimension of the measurement space equals the number of recording sites.

Let E_p be the p-dimensional phase-space of the system and E_m the m-dimensional measurement space. In the following, $(\mathbf{e_1}, \mathbf{e_2}, \ldots, \mathbf{e_p})$ and $(\mathbf{f_1}, \mathbf{f_2}, \ldots, \mathbf{f_m})$ denote the natural basis of E_p and E_m.

To any state $\boldsymbol{\chi} \in E_p$, corresponds unambiguously a set of measures $\mathbf{y} \in E_m$ given by:

$$\mathbf{y} = A \cdot \boldsymbol{\chi}$$

where A is the (m, p) transmission matrix of the source-to-scalp coefficients. It is easily computed from the positions and orientations of the dipoles and the electrode locations [de Munck, 1988]. Let's denote $(\boldsymbol{\lambda}_1, \boldsymbol{\lambda}_2, \ldots, \boldsymbol{\lambda}_m)$ the m rows of A, $(\boldsymbol{\lambda}_i \in R^p)$. These m vectors define an r-dimensional subspace of R^p $(r < \inf(m, p))$ from which it is possible to build an orthonormal basis $(\boldsymbol{\mu}_1, \boldsymbol{\mu}_2, \ldots, \boldsymbol{\mu}_r)$, that is part of an orthonormal basis of R^p: $(\boldsymbol{\mu}_1, \boldsymbol{\mu}_2, \ldots, \boldsymbol{\mu}_p)$. Let's then denote $\boldsymbol{H}$ the (m, p) matrix, such that

$$\boldsymbol{\lambda}_j = \sum_{i=1\to r} H_{lj}\boldsymbol{\mu}_l$$

for $j \in (1, m)$ and R the (p, p) orthogonal matrix, such that

$$\mathbf{e_i} = \sum_{k=1\to p} R_{ki}\boldsymbol{\mu}_k,$$

for $i \in (1, p)$.

Any state-space vector can be written:

$$\boldsymbol{\chi} = \sum_{i=1\to p} \chi_i \mathbf{e_i} = \sum_{i=1\to p} \chi_i \left(\sum_{k=1\to p} R_{ki}\boldsymbol{\mu}_k \right) = \sum_{k=1\to p} \left(\sum_{i=1\to p} \chi_i R_{ki} \right) \boldsymbol{\mu}_k$$

since the corresponding measurements vector is given by:

$$\mathbf{y} = A \cdot \boldsymbol{\chi} = \sum_{j=1\to m} ({}^t\Lambda_j \cdot \boldsymbol{\chi})\mathbf{f_j} = \sum_{j=1\to m} \left(\sum_{l=1\to r} H_{lj}{}^t \boldsymbol{\mu}_l \cdot \boldsymbol{\chi} \right) \mathbf{f_j}$$

$$\mathbf{y} = \sum_{j=1\to m} \left(\sum_{l=1\to r} H_{lj}{}^t \boldsymbol{\mu}_l \cdot \left(\sum_{k=1\to p} \left(\sum_{i=1\to p} x_i R_{ki} \right) \boldsymbol{\mu}_k \right) \right) \mathbf{f_j}$$

$$= \sum_{j=1\to m} \left(\sum_{l=1\to r} \left(\sum_{k=1\to p} \left(\sum_{i=1\to p} H_{lj}{}^t \boldsymbol{\mu}_l x_i R_{ki} \boldsymbol{\mu}_k \right) \right) \right) \mathbf{f_j}$$

and since $(\boldsymbol{\mu}_1, \boldsymbol{\mu}_2, \ldots, \boldsymbol{\mu}_p)$ is orthonormal:

$$y_j = \sum_{i=1\to p} \left(\sum_{k=1\to p} H_{kj} R_{ki} \right) \chi_i,$$

for all $j \in (1, m)$ and $\mathbf{y} = {}^t\mathbf{H} \cdot R \cdot \boldsymbol{\chi}$.

This formula gives us precise information about the geometric transformation leading from $\boldsymbol{\chi}$ to $\mathbf{y}$, and thus, from the phase-space trajectory (let's denote it T) to the reconstructed trajectory (T′). Since R is orthogonal, it corresponds to a rotation ρ in the phase-space, and thus:

1. T is rotated (Fig. 9) using the transformation ρ, that brings $\boldsymbol{\mu}_j$ on $\mathbf{e_j}$ for all $j \in (1, p)$.
2. The resulting curve $\rho(T)$ is then projected down to the subspace $\langle \mathbf{e_1}, \mathbf{e_2}, \ldots, \mathbf{e_r} \rangle$ (let's denote this projection π).
3. If t denotes the transformation that transforms $\boldsymbol{\mu}_j$ on $\boldsymbol{\lambda}_j$ for all $j \in (1, r)$, then the projection of T′ on the i-th axis of E_m is given by the projection of $(\pi O \rho)(T)$ on $\tau(\mathbf{e}_j)$.

Although complex in appearance, this procedure leads to a straightforward conclusion concerning the relations between the topological properties of T and T′.

Lemma

If the diffusion matrix A is known and the transformations ρ, π, and τ have been constructed using families of vectors $(\boldsymbol{\lambda_1}, \boldsymbol{\lambda_2}, \ldots, \boldsymbol{\lambda_m})$ and $(\boldsymbol{\mu_1}, \boldsymbol{\mu_2}, \ldots, \boldsymbol{\mu_p})$, then in the case of the multichannel reconstruction, two points M and P of the phase-space trajectory T have the same image on the reconstructed trajectory T′, if and only if the following proposition is true:

$$\rho(MP) \in (\langle \mathbf{e_1}, \ldots, \mathbf{e_r} \rangle)^{\perp} \text{ (or } \mathbf{MP} \in \langle \boldsymbol{\mu}_{r+1}, \ldots, \boldsymbol{\mu}_p \rangle).$$

Notice that the single-channel case can be easily deduced, for in this case two segments of T, $(M_1, M_2, \ldots, M_m)$ and $(P_1, P_2, \ldots, P_m)$, will result in the same point on T′, if the following proposition is true: each of the projections of the vectors $\rho(M_i P_i)$ is either zero, or perpendicular to $\tau(\mathbf{e}_\alpha)$ where α denotes the recording channel.

This lemma makes it possible to derive a sufficient condition that ensures the topological identity between the phase-space trajectory and the reconstructed one, it is presented in the following corollary.

Corollary

Assuming the number of recording sites exceeds the size of the phase-space (i.e., $m > p$), and assuming that the diffusion matrix A is injective (a signal can be recorded on the scalp if at least one of the dipoles has an amplitude different from zero), then $r = p$,

$\langle \mathbf{e_1}, \ldots, \mathbf{e_r} \rangle^{\perp} = \{0\}$. Thus two points of T cannot have the same image on T′, and it follows that the correspondence between T and T′ is one to one.

APPENDIX B

In this appendix, we study the effect of average reference on the reconstruction of dynamics.

With the same notations as in the previous appendix, we compute from the activities $\mathbf{x} \in E_p$ of the dipoles, the set of scalp potentials $\underline{y} \in E_m$ given by:

$$\mathbf{y} = \mathbf{A} \cdot \mathbf{x}.$$

If we subtract the average reference, we obtain a set of data

$$\mathbf{z} = \mathbf{y} - (1/n) \cdot (\mathbf{y} \cdot \mathbf{e})\mathbf{e},$$

where n is the size of **y** and $\mathbf{e} = (1, 1, 1, \ldots, 1, 1)$ of size n. **z** is the orthogonal projection **P** (i.e., that $\mathbf{z} \cdot \mathbf{e} = 0$) of **y** onto the $(n - 1)$-dimensional space $\langle e \rangle^{\perp}$: $\mathbf{z} = \mathbf{P} \cdot \mathbf{y} = \mathbf{P} \cdot \mathbf{A} \cdot \mathbf{x}$.

In the following paragraph, we show that **z** can also be written $\mathbf{z} = \mathbf{A} \cdot \mathbf{Q} \cdot \mathbf{x}$, where **Q** is a projection. Since the projection acts now on the original dipole set **x**, it follows that average reference induces a *modified* dipole source.

The state-space E_p can be written as the orthogonal sum of two subspaces:

$$E_p = \mathrm{Ker}(\mathbf{A}) \overset{\perp}{\oplus} \prod,$$

and further it can be shown that:

$$\prod = \left(\prod \cap \mathrm{Ker}(\mathbf{P} \cdot \mathbf{A})\right) \oplus \left(\prod \cap \mathrm{Ker}(\mathbf{P} \cdot \mathbf{A} - \mathbf{A})\right).$$

Let's briefly demonstrate this point.

1. The first step is to show that the intersection of the two subspaces

$$\left(\prod \cap \mathrm{Ker}(\mathbf{P} \cdot \mathbf{A})\right) \cap \left(\prod \cap \mathrm{Ker}(\mathbf{P} \cdot \mathbf{A} - \mathbf{A})\right)$$

is zero. If $\mathbf{u} \in (\Pi \cap \mathrm{Ker}(\mathbf{P} \cdot \mathbf{A})) \cap (\Pi \cap \mathrm{Ker}(\mathbf{P} \cdot \mathbf{A} - \mathbf{A}))$, then $\mathbf{P} \cdot \mathbf{A} \cdot \mathbf{u} = \mathbf{0}$, and $\mathbf{P} \cdot \mathbf{A} \cdot \mathbf{u} = \mathbf{A} \cdot \mathbf{u}$; so

$$\mathbf{A} \cdot \mathbf{u} = \mathbf{0} \quad \text{and} \quad \mathbf{u} \in \left(\prod \cap \mathrm{Ker}(\mathbf{A})\right) = \{0\},$$

so $\mathbf{u} = \mathbf{0}$. Thus

$$\left(\prod \cap \mathrm{Ker}(\mathbf{P} \cdot \mathbf{A})\right) \cap \left(\prod \cap \mathrm{Ker}(\mathbf{P} \cdot \mathbf{A} - \mathbf{A})\right) = \{0\}.$$

2. The second step is to show that every element of Π can be written as the sum of two vectors, each belonging to one of the subspaces $(\Pi \cap \mathrm{Ker}(\mathbf{P} \cdot \mathbf{A}))$ and $(\Pi \cap \mathrm{Ker}(\mathbf{P} \cdot \mathbf{A} - \mathbf{A}))$. If $\mathbf{u} \in \Pi$, then $\mathbf{A} \cdot \mathbf{ue}$ can be written

$$\mathbf{A} \cdot \mathbf{u} = \mathbf{g} + \lambda \cdot \mathbf{e},$$

where λ is a scalar and $\mathbf{g} \in \langle e \rangle^{\perp}$. Let **k** be a vector such that

$$\mathbf{A} \cdot \mathbf{k} = \mathbf{e} \left(\text{then } \mathbf{k} \in \left(\prod \cap \mathrm{Ker}(\mathbf{P} \cdot \mathbf{A})\right)\right),$$

u can always be written:

$$\mathbf{u} = \lambda \cdot \mathbf{k} + (\mathbf{u} - \lambda \cdot \mathbf{k}). \quad \text{Then,}$$

$$\mathbf{P} \cdot \mathbf{A} \cdot (\mathbf{u} - \lambda \cdot \mathbf{k}) = \mathbf{P} \cdot (\mathbf{A} \cdot \mathbf{u} - \lambda \mathbf{e}) = \mathbf{P} \cdot \mathbf{g} = \mathbf{g} = \mathbf{A} \cdot (\mathbf{u} - \lambda \cdot \mathbf{k}); \quad \text{so}$$

$$(\mathbf{u} - \lambda \cdot \mathbf{k}) \in \left(\prod \cap \mathrm{Ker}(\mathbf{P} \cdot \mathbf{A} - \mathbf{A})\right) \text{ and thus}$$

$$\mathbf{u} \in \left(\prod \cap \mathrm{Ker}(\mathbf{P} \cdot \mathbf{A})\right) \oplus \left(\prod \cap \mathrm{Ker}(\mathbf{P} \cdot \mathbf{P} - \mathbf{A})\right). \quad \text{Thus}$$

$$\prod \subset \left(\prod \cap \mathrm{Ker}(\mathbf{P} \cdot \mathbf{A})\right) \oplus \left(\prod \cap \mathrm{Ker}(\mathbf{P} \cdot \mathbf{A} - \mathbf{A})\right) \subset \prod.$$

Now let **Q** be the projection onto

$$\left(\prod \cap \mathrm{Ker}(\mathbf{P} \cdot \mathbf{A} - \mathbf{A})\right).$$

Since

$$E_p = \mathrm{Ker}(\mathbf{A}) \oplus \left(\prod \cap \mathrm{Ker}(\mathbf{P} \cdot \mathbf{A})\right) \oplus \left(\prod \cap \mathrm{Ker}(\mathbf{P} \cdot \mathbf{A} - \mathbf{A})\right),$$

any vector $\mathbf{u}$ of E_p can be written

$$\mathbf{u} = \mathbf{u_a} + \mathbf{u_b} + \mathbf{u_c},$$

with

$$\mathbf{u_a} \in \mathrm{Ker}(\mathbf{A}), \quad \mathbf{u_b} \in \left(\prod \cap \mathrm{Ker}(\mathbf{P} \cdot \mathbf{A})\right),$$

and

$$\mathbf{u_c} \in \left(\prod \cap \mathrm{Ker}(\mathbf{P} \cdot \mathbf{A} - \mathbf{A})\right)(\mathbf{u_c} = \mathbf{Q} \cdot \mathbf{u}).$$

Then,

$$\mathbf{P} \cdot \mathbf{A} \cdot \mathbf{u} = \mathbf{P} \cdot \mathbf{A} \cdot (\mathbf{u_a}) + \mathbf{P} \cdot \mathbf{A} \cdot (\mathbf{u_b}) + \mathbf{P} \cdot \mathbf{A} \cdot (\mathbf{u_c}))$$
$$= \mathbf{P}(\mathbf{o}) + \mathbf{o} + \mathbf{u_c} = \mathbf{u_c}.$$

Since

$$\mathbf{u_c} = \mathbf{Q} \cdot \mathbf{u},$$

then it is true that

$$\mathbf{P} \cdot \mathbf{A} \cdot \mathbf{u} = \mathbf{A} \cdot \mathbf{Q} \cdot \mathbf{u}.$$

It follow that, as announced, $\mathbf{z}$ can also be written

$$\mathbf{z} = \mathbf{A} \cdot \mathbf{Q} \cdot \mathbf{x},$$

where $\mathbf{Q}$ is a projection. $\mathbf{Q}$ is the potential generated by the set of dipoles when their activity is $\mathbf{x}' = \mathbf{Q} \cdot \mathbf{x}$, a modified dipole source instead of the original one.

For this reason, the *average reference* should be used with care, since there may be important differences between $\mathbf{x}'$ and $\mathbf{x}$ and between their dynamics.